Transaction A: Civil Engineering
Vol. 17, No. 5, pp. 372–386

SCIENTIA IRANICA

3D Modeling of Damage Growth and Crack Initiation Using Adaptive Finite Element Technique

H. Moslemi[1] and A.R. Khoei[1,*]

Abstract. *In this paper, the continuum damage mechanics model originally proposed by Lemaitre (Journal of Engineering Materials and Technology. 1985; 107: 83-89) is presented through an adaptive finite element method for three-dimensional ductile materials. The macro-crack initiation-propagation criterion is used based on the distribution of damage variable in the continuum damage model. The micro-crack closure effect is incorporated to simulate the damage evolution more realistic. The Zienkiewicz-Zhu posteriori error estimator is employed in conjunction with a weighted Superconvergence Patch Recovery (SPR) technique at each patch to improve the accuracy of error estimation and data transfer process. Finally, the robustness and accuracy of proposed computational algorithm is demonstrated by several 3D numerical examples.*

Keywords: *Damage mechanics; Crack initiation; Crack closure; Adaptive mesh refinement; Weighted SPR technique.*

INTRODUCTION

The fracture of ductile materials is the consequence of a progressive damaging process and considerable plastic deformation usually precedes the ultimate failure. The numerical prediction of damage evolution and crack initiation-propagation can be described by the means of continuum damage approach. The continuum damage mechanics was originally developed to describe the creep rupture. It was first introduced by Kachanov [1] to describe the effects of an isotropic distribution of spherical voids on plastic flow. Rice and Tracy [2] analytically investigated the evolution of spherical voids in an elastic-perfectly plastic matrix. Gurson [3] proposed a model based on the theory of elasto-plasticity for ductile damage where the (scalar) damage variable was obtained from the consideration of microscopic spherical voids embedded in an elasto-plastic matrix. It was shown that the theory is particularly suitable for representation of the behavior of porous metals. Murakami and Ohno [4] proposed a second-rank symmetric tensor for the anisotropic damage variable in which the definition of damage variable follows from the extension of effective stress concept to three-dimensions by means of the hypothesis of the existence of a mechanically equivalent fictitious undamaged configuration. Lemaitre [5] proposed a micro-mechanical damage model to simulate the physical process of void nucleation, growth and coalescence using continuum mechanics. An anisotropic theory of continuum damage mechanics was developed by Chow and Wang [6] for ductile fracture in which the anisotropic damage evolution characterized by a generalized damage characteristic tensor. Lemaitre and Chaboche [7] pointed out the fracture as the ultimate consequence of material degradation process.

The conventional continuum damage descriptions of material degeneration suffer from the loss of well-posedness beyond a certain level of accumulated damage. Peerlings et al. [8] introduced the higher-order deformation gradient in the constitutive model to improve the deficiency of standard damage models. Pardoen [9] proposed an extended Gurson model to encompass both the low and large stress triaxiality regimes. A comparison between the Lemaitre and Gurson damage models was performed by Hambli [10] in crack growth

1. *Center of Excellence in Structures and Earthquake Engineering, Department of Civil Engineering, Sharif University of Technology, Tehran, P.O. Box 11155-9313, Iran.*
*. *Corresponding author. E-mail: arkhoei@sharif.edu*

Received 28 February 2010; received in revised form 18 May 2010; accepted 9 August 2010

simulation and demonstrated that the Gurson damage model cannot predict the fracture propagation path in a realistic way while the Lemaitre model gives good results. Areias and Belytschko [11] coupled the continuum damage constitutive model with the X-FEM formulation to model the crack initiation and propagation. Grassl and Jirasek [12] combined the stress-based plasticity and strain-driven scalar damage to model the failure of concrete. Mediavilla et al. [13] simulated the ductile damage and fracture in metal forming processes using a combined continuous-discontinuous approach which accounts for the interaction between macroscopic cracks and the surrounding softening material. A transition from continuum damage to cohesive crack propagation was developed by Comi et al. [14] in concrete structures via the X-FEM technique. The aim of present study is to model the fracture of ductile materials using an adaptive FE mesh refinement technique.

Adaptive finite element method utilizes the error estimation to assess the quality of results and modify the mesh during the solution, aiming to achieve approximate solution within some bounds from the exact solution of continuum problem. An overview of various error estimation techniques was presented by Verfurth [15] for elasticity problems. Error estimators can be basically divided into two categories. A priori error estimation, which is based on the knowledge of characteristics of the solution, provides qualitative information about the asymptotic rate of convergence as the number of degrees of freedom goes to infinity [16]. A posteriori error estimation employs the solution obtained by the numerical analysis, in addition to a priori assumptions about the solution [17]. Babuska and Rheinboldt [18] proposed a residual based method of error estimation which considers local residuals of the numerical solution. The recovery technique is an alternative approach which computes an improved solution using a recovery process in which the error is simply estimated as the difference between the recovered solution and numerical solution [19]. Various recovery procedures were proposed in the literature in which the superconvergent patch recovery method is one of the most effective ones.

The Superconvergent Patch Recovery (SPR) method was first introduced by Zienkiewicz and Zhu [19,20] in linear elastic problems. The technique was applied in nonlinear analysis by Boroomand and Zienkiewicz [21] in which the strain was recovered by SPR in elasto-plasticity problems. The SPR method was proposed by Wiberg et al. [22] to improve the accomplishment of equilibrium equations and the boundary conditions applied to the smoothed stresses. A modified SPR method was applied by Gu et al. [23] to improve the accuracy and stability of the technique by introducing additional nodal points. Bugeda [24] proposed an enriched SPR method based on the sensitivity analysis for better estimation of error. An extension of SPR technique to 3D plasticity problems was presented by Khoei and Gharehbaghi [25,26]. A modified-SPR technique was applied by Khoei et al. [27] for simulation of crack propagation in which the polynomial function was replaced by singular terms of analytical solution of crack problems in the process of recovery solution. The technique was improved by Moslemi and Khoei [28] and Khoei et al. [29] to estimate a more realistic error in LEFM problems and cohesive zone models by applying the weighting function for various sampling points.

In the present paper, an adaptive finite element method is presented based on the weighted-SPR technique to model the damage of ductile material in 3D problems. The Lemaitre damage model is employed and the micro-crack closure effect is incorporated to simulate the damage evolution. The macro-crack initiation-propagation criterion is used based on the distribution of damage variable. The plan of the paper is as follows: The Lemaitre damage model and its implementation in finite element context are described together with the crack closure effect. The error estimation based on weighted-SPR method is then presented along with the adaptive mesh refinement and data transfer process. Finally, the robustness and accuracy of computational algorithm are demonstrated by several numerical examples.

NONLINEAR DAMAGE MODEL

Damage in materials is mainly the process of initiation and growth of micro-cracks and cavities. Continuum damage mechanics discusses systematically the effects of damage on the mechanical properties of materials and structures as well as the influence of external conditions and damage itself on the subsequent development of damage. In this study, this nonlinear interaction is investigated via the Lemaitre damage constitutive model. In order to describe the internal degradation of solids within the framework of the continuum mechanics theory, new variables intrinsically connected with the internal damage process need to be introduced in addition to the standard variables. Variables of different mathematical nature possessing different physical meaning have been employed in the description of damage under various circumstances. The damage variable used here is the relative area of micro-cracks and intersections of cavities in any plane oriented by its normal $\mathbf{n}$ as [30]:

$$D_{(\mathbf{n})} = \frac{S_\Phi}{S}, \tag{1}$$

where S_Φ is the area of micro-cracks and intersections and S is the total area of the cross section as shown in Figure 1. It is assumed that micro-cracks and

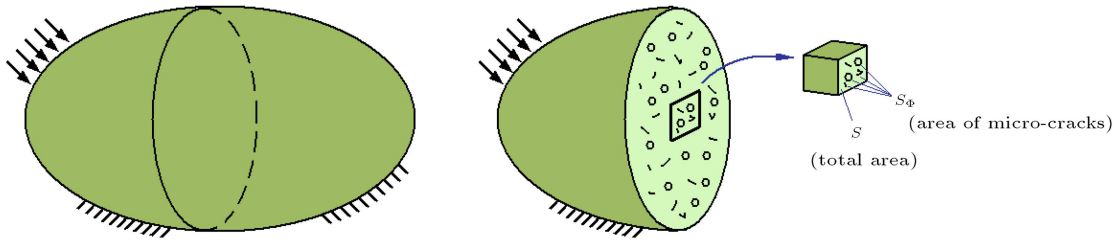

Figure 1. A damaged element presenting the areas S and S_Φ.

cavities are distributed uniformly in all directions. In the isotropic case, the damage variable is adopted as a scalar. The behavior of damaged material is governed by the principle of strain equivalence which states that the strain behavior of a damaged material is represented by constitutive equations of the virgin material (without damage) in the potential of which the stress is simply replaced by the effective stress. By this assumption the effective stress tensor is related to the true stress tensor by:

$$\boldsymbol{\sigma}_{\text{eff}} = \frac{1}{1-D}\boldsymbol{\sigma}. \tag{2}$$

Consider Y be the thermodynamic variable associated with the damage variable D as:

$$Y = \frac{\partial u}{\partial D} = -\frac{1}{2}\boldsymbol{\varepsilon}^e : \mathbf{D}^e : \boldsymbol{\varepsilon}^e, \tag{3}$$

where ':' denoted component by component product of tensors. This quantity is called damage energy release rate and is expanded by using the inverse of the elastic stress-strain law as:

$$\begin{aligned} Y &= -\frac{1}{2(1-D)^2}\boldsymbol{\sigma} : [\mathbf{D}^e]^{-1} : \boldsymbol{\sigma} \\ &= -\frac{1}{2E(1-D)^2}[(1+\nu)\boldsymbol{\sigma} : \boldsymbol{\sigma} - \nu(tr\boldsymbol{\sigma})^2] \\ &= -\frac{q^2}{2E(1-D)^2}\left[\frac{2}{3}(1+\nu) + 3(1-2\nu)\left(\frac{p}{q}\right)^2\right], \end{aligned} \tag{4}$$

where p is the hydrostatic stress and q is the equivalent von-Mises stress. In Lemaitre damage model the evolution of damage variable is assumed to be given by:

$$\dot{D} = \begin{cases} 0 & \varepsilon^p_{eq} \le \varepsilon^p_D \\ \dot{\gamma}\frac{1}{1-D}\left(\frac{-Y}{r}\right)^s & \varepsilon^p_{eq} > \varepsilon^p_D \end{cases} \tag{5}$$

where r and s are material and temperature-dependant properties, $\varepsilon^p_{eq} = \sqrt{2/3\|\boldsymbol{\varepsilon^p}\|}$ is equivalent plastic strain, $\dot{\gamma}$ is the plastic multiplier and is equal to the rate of equivalent plastic strain and ε^p_D is threshold damage where damage growth starts only at this critical value. As can be seen in above equation, the damage rate depends on the stress state, plastic strain growth and instantaneous damage variable. The effect of damage variable on mechanical behavior of material is accounted in degradation of elastic modulus of material and its yield surface. Based on the equivalent strain principle, this modification can be expressed as:

$$\mathbf{D}_{\text{eff}} = (1-D)\mathbf{D}^e, \tag{6}$$

$$\Phi = \sqrt{\frac{3}{2}}\frac{\|\mathbf{s}\|}{(1-D)} - [\sigma^0_Y + R(\varepsilon^p_{eq})], \tag{7}$$

where $\mathbf{D}^e$ and $\mathbf{D}_{\text{eff}}$ are the elastic modulus of material before damage and after damage, respectively, Φ is the modified yield surface, $\mathbf{s}$ is the deviatoric stress tensor and R is the isotropic plastic growth function. In a damaged medium, three distinctive regions can be recognized (Figure 2): firstly, the region S_0 where no damage has been occurred, secondly, the region S_d where the damage is sub-critical and only degrades the material, and finally, the region S_C where the damage variable is reached the critical value D_C. If the critical damage value is satisfied within an element, the element fractures and cracks occur.

Finite Element Implementation

The accuracy of the overall finite element scheme depends crucially on the accuracy of particular numerical algorithm adopted. This section describes a numerical procedure for integration of the Lemaitre damage elasto-plastic model, presented in preceding section,

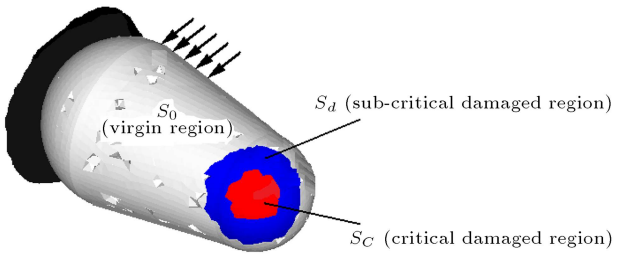

Figure 2. Damaged zones in a schematic model.

based on the well-known two-step elastic predictor-plastic corrector method [31]. At each Gauss point, the values of state variables including the stress tensor $\boldsymbol{\sigma}_n$, plastic strain tensor $\boldsymbol{\varepsilon}^p_n$, equivalent plastic strain $(\varepsilon^p_{eq})_n$ and damage variable D_n are known at the start of interval, and for a given strain increment $\boldsymbol{\Delta\varepsilon}$, the value of variables are desired at the end of interval. At the first stage of computational algorithm the material behavior is assumed to be elastic; the yield surface at the end of interval can be then evaluated as:

$$\Phi = \sqrt{\frac{3}{2}}\frac{\|\mathbf{s}_{n+1}\|}{(1-D_n)} - [\sigma^0_Y + R(\varepsilon^p_{eq})_n]. \tag{8}$$

If $\Phi \leq 0$, the assumed elastic behavior is correct and the damage variable and plastic strain remain unchanged. If $\Phi > 0$, the plastic corrector step must be applied to obtain the updated state variables by simultaneously establishing four equations consisting of the plastic flow equation, equivalent plastic strain growth equation, damage growth equation and the yield surface equation as:

$$\boldsymbol{\varepsilon}^p_{n+1} = \boldsymbol{\varepsilon}^p_n + \frac{\Delta\gamma}{1-D_{n+1}}\sqrt{\frac{3}{2}}\frac{\mathbf{s}_{n+1}}{\|\mathbf{s}_{n+1}\|}, \tag{9}$$

$$(\varepsilon^p_{eq})_{n+1} = (\varepsilon^p_{eq})_n + \Delta\gamma, \tag{10}$$

$$D_{n+1} = D_n + \Delta\gamma\frac{1}{1-D_{n+1}}\left(\frac{-Y_{n+1}}{r}\right)^s, \tag{11}$$

$$\Phi = \sqrt{\frac{3}{2}}\frac{\|\mathbf{s}_{n+1}\|}{(1-D_{n+1})} - [\sigma^0_Y + R(\varepsilon^p_{eq})_{n+1}] = 0. \tag{12}$$

The solution of these four nonlinear coupled equations simultaneously is a costly computational task. Steinmann et al. [32] presented that by performing relatively straightforward algebraic manipulations, the above system can be reduced to a single nonlinear algebraic equation for the plastic multiplier $\Delta\gamma$ expressed as:

$$\omega(\Delta\gamma) - \omega_n + \frac{\Delta\gamma}{\omega(\Delta\gamma)}\left(\frac{-Y(\Delta\gamma)}{r}\right)^s = 0, \tag{13}$$

where ω is the integrity variable in contrast to damage variable and is evaluated by:

$$\begin{aligned}\omega_{n+1} &= 1 - D_{n+1} = \omega(\Delta\gamma)\\ &= \frac{3G\Delta\gamma}{\bar{q}^{\text{trial}}_{n+1} - \sigma_Y(R_n + \Delta\gamma)},\end{aligned} \tag{14}$$

where $\bar{q}^{\text{trial}}_{n+1}$ is the von-Mises equivalent stress obtained by the elastic predictor step. The damage energy release rate is a function of $\Delta\gamma$ calculated by:

$$Y(\Delta\gamma) = \frac{[\sigma_Y(R_n + \Delta\gamma)]^2}{6G} + \frac{\bar{p}^2_{n+1}}{2K}, \tag{15}$$

where $\bar{p}_{n+1}$ is the elastic predicted hydrostatic pressure without damage effect. Equation 13 can be solved by an iterative method such as Newton-Raphson method. An initial guess is very effective in the rate of convergence of the method. In this study, the following initial guess proposed by de Souza Neto et al. [33] is employed as:

$$\Delta\gamma^{(0)} = \frac{[\bar{q}^{\text{trial}}_{n+1} - \sigma_Y(R_n)]\omega_n}{3G}. \tag{16}$$

It was shown that the above initial guess reduces the total number of iterations required for convergence, as compared to the usual choice of $\Delta\gamma^{(0)} = 0$. By computing the plastic multiplier, the updated state variables can be obtained using four basic equations.

Micro-Crack Closure Effect

From the micromechanical view, the damage can be considered as the degradation of material properties due to the evolution of voids and micro-cracks. The Lemaitre damage model discussed in the previous section suffers from an important drawback, since the effect of hydrostatic stress is captured by the damage energy release rate Y with equal response in tension and compression. On the other hand, the micro-cracks which open in tensile stresses may partially close at a compression stress state. Hence, after having been damaged in tension, the material recovers its stiffness partially under compression. To remedy this problem, several decompositions are proposed, such as the elastic energy decomposition [34], the Kelvin decomposition of compliance tensor [35], the damage tensor decomposition [36], or more classically based on the stress tensor decomposition into a positive and negative part [37-40]. In this study, the stress tensor is decomposed into the positive and negative parts and the effect of compressive stress tensor is considered a fraction of the effect of tensile stress tensor. In the process of decomposition, the stress tensor is first mapped to the principle directions to form a diagonal matrix with the principle stresses. This matrix is then decomposed to tensile and compressive stress tensors as:

$$\sigma = \sigma^+ + \sigma^-. \tag{17}$$

This decomposition is defined mathematically using the Macaulay bracket $\langle\ \rangle$ as:

$$\boldsymbol{\sigma}^+ = \begin{bmatrix}\langle\sigma_1\rangle & 0 & 0\\ 0 & \langle\sigma_2\rangle & 0\\ 0 & 0 & \langle\sigma_3\rangle\end{bmatrix},$$

$$\boldsymbol{\sigma}^- = -\begin{bmatrix}\langle-\sigma_1\rangle & 0 & 0\\ 0 & \langle-\sigma_2\rangle & 0\\ 0 & 0 & \langle-\sigma_3\rangle\end{bmatrix}. \tag{18}$$

The Macaulay bracket is a scalar function defined as:

$$\langle a \rangle = \begin{cases} a & \text{if } a \geq 0 \\ 0 & \text{if } a < 0 \end{cases} \tag{19}$$

By decomposition of stress tensor, each component affects the damage energy release rate separately. The effect of tensile component given in previous section remains valid, but the compression component has a more moderate effect with an experimental reduction factor of h, which can be determined by the technique proposed by Arnold et al. [41]. This value is called the crack closure effect constant and has the value in the range of $[0-1]$. At the extreme values, $h=0$ implies the full crack closure and $h=1$ represents the damage model without crack closure effect. Thus, the effect of compressive component of stress tensor can be superposed with the effect of tensile component of stress tensor by modifying Equation 4 as:

$$Y = -\frac{1}{2E(1-D)^2}[(1+\nu)\boldsymbol{\sigma}^+ : \boldsymbol{\sigma}^+ - \nu\langle tr\boldsymbol{\sigma}\rangle^2] - \frac{h}{2E(1-hD)^2}[(1+\nu)\boldsymbol{\sigma}^- : \boldsymbol{\sigma}^- - \nu\langle -tr\boldsymbol{\sigma}\rangle^2]. \tag{20}$$

By modifying the value of damage energy release rate, the remaining parts of the procedure of original Lemaitre model will not be changed.

ADAPTIVE FE STRATEGY

In numerical analysis of FE solution, it is essential to introduce some measures of error and use adaptive mesh refinement to keep this error within prescribed bounds to ensure that the finite element method is effectively used for practical analysis. To automate this process, adaptive finite elements have been implemented to obtain an optimal mesh. Most of the pioneering mathematical works, such as Babuska and Rheinboldt [18], Zienkiewicz and Zhu [19, 20], Gago et al. [42] and Kelly et al. [43], have been today translated into engineering usage. Due to the localized material deterioration in the damaged body problems, many elements will be severely distorted producing unacceptably inaccurate solutions and this optimization takes a more important and necessary role. In order to obtain an optimal mesh, in the sense of an equal solution quality, it is desirable to design the mesh such that the error contributions of the elements are equally distributed over the mesh. This criterion illustrates what parts of the discretized domain have to be refined/de-refined and what degree of mesh fineness is needed to maintain the solution error within the prescribed bounds. The plastic deformation of problem necessitates transferring all relevant variables from the old mesh to new one. In general, the procedure described above can be executed in four parts: an error estimation, an adaptive mesh refinement, an adaptive mesh generator, and the mapping of variables.

Error Estimation Using Weighted SPR Technique

In damage mechanics problems, the damage variable plays an important role in predicting the crack initiation and crack growth. Thus, the error needs to be estimated based on the damage variable D, i.e. $e_D = D - \widehat{D}$, with D denoting the exact value of damage variable and $\widehat{D}$ the damage value derived by a finite element solution. Since the exact value of damage variable is not available, a recovered solution is used instead of exact one and then approximate the error as the difference between the recovered values and that given directly by the finite element solution, i.e. $e_D \approx D^* - \widehat{D}$, where D^* denotes the recovered value of damage variable D. In order to obtain an improved solution, the nodal smoothing procedure is performed using the Weighted Superconvergent Patch Recovery (WSPR) technique, which was originally proposed by Moslemi and Khoei [28] to simulate the crack growth in linear fracture mechanics. The objective of recovery of the FE solution is to obtain the nodal values of damage variable D such that the smoothed continues field defined by the shape functions and nodal values is more accurate than that of the finite element solution.

A procedure for utilizing the Gauss quadrature values is based on the smoothing of such values by a polynomial of order p in which the number of sample points can be taken as greater than the number of parameters in the polynomial. The recovered solution of damage variable D^* can be obtained as $D^* = \mathbf{Pa}$, with $\mathbf{a}$ denoting a vector of unknowns assumed as:

$$\mathbf{a} = \langle a_1, a_2, a_3, a_4 \rangle^T,$$

and $\mathbf{P}$ the polynomial base functions given by:

$$\mathbf{P} = \langle 1, x, y, z \rangle.$$

The determination of the unknown parameters $\mathbf{a}$ can be made by performing a least square fit to the values of superconvergent or sampling points. After finite element analysis, a patch is defined for each vertex node inside the domain by the union of elements sharing the node. At each node of interior patch center, the connected tetrahedral elements along with their nodes and Gauss points are obtained. In the standard SPR technique, all sampling points have similar properties in the patch, which may produce significant errors in the boundaries, particularly the edges of crack. In fact, for elements located on the boundaries or crack edges,

which do not have enough sampling points, we need to use the sampling points of nearest patch. These new sampling points induce unreal value of damage variables in the patch and overestimate the value of error, which results in unreasonable mesh refinement in the boundaries of domain. Moslemi and Khoei [28] proposed the weighted-SPR technique by using different weighting parameters for sampling points of the patch. It results in more realistic recovered values at the nodal points, particularly near the crack tip and boundaries. Hence, if we have n sampling points in the patch with the coordinates (x_k, y_k, z_k), the function F needs to be minimized in this patch as:

$$F(\mathbf{a}) = \sum_{k=1}^{n} w_k [D_i^*(x_k, y_k, z_k) - \widehat{D}_i(x_k, y_k, z_k)]^2$$

$$= \sum_{k=1}^{n} w_k [\mathbf{P}(x_k, y_k, z_k)\mathbf{a} - \widehat{D}_i(x_k, y_k, z_k)]^2. \quad (21)$$

In order to incorporate the effects of nearest sampling points in the recovery process, the weighting parameter is defined as $w_k = 1/r_k$, with r_k denoting the distance of sampling point from the vertex node which is under recovery. The minimization of function F with respect to $\mathbf{a}$ results in the unknown parameters $\mathbf{a}$ as:

$$\mathbf{a} = \left(\sum_{k=1}^{n} w_k^2 \mathbf{P}_k^T \mathbf{P}_k \right)^{-1} \sum_{k=1}^{n} \left[w_k^2 \mathbf{P}_k^T \widehat{D}_i(x_k, y_k) \right]. \quad (22)$$

Once the components of the vector of unknown parameters $\mathbf{a}$ are determined, the damage variables at nodal points inside the patch are computed by using the interpolation of the shape functions. These nodal values $\bar{\mathbf{D}}^*$ can be used to construct a continuous damage field over the entire domain at the next step, that is, for each element, the recovered damage variable is represented as an interpolation of nodal values using the standard shape functions $\mathbf{N}$ in finite element analysis as $D^* = \mathbf{N}\bar{\mathbf{D}}^*$. The recovered damage variable obtained by this relation can be used to obtain a pointwise error in the domain. Since the pointwise error becomes locally infinite in critical points, such as crack tip, the error estimator can be replaced by a global parameter using the norm of error defined as:

$$\|e_D\| = \|D^* - \widehat{D}\| = \left(\int_\Omega (D^* - \widehat{D})^T (D^* - \widehat{D}) d\Omega \right)^{1/2}. \quad (23)$$

The above L_2 norm is defined over the whole domain Ω. The overall error can be related to each element error by:

$$\|e_D\|^2 = \sum_{i=1}^{m} \|e_D\|_i^2,$$

with i denoting an element contribution and m the total number of elements. The distribution of error norm across the domain indicates which portions need refinement and which other parts need de-refinement, or coarsening elements. Since the total error permissible must be less than a certain value, it is a simple matter to search the design field for a new solution in which the total error satisfies this requirement. In fact, after remeshing each element must obtain the same error and the overall percentage error must be less than the target percentage error, i.e.:

$$\theta = \|e_D\| / \|\widehat{D}\| \leq \theta_{\text{aim}} = \|e_D\|_{\text{aim}} / \|\widehat{D}\|,$$

with θ_{aim} denoting the prescribed target percentage error. Hence, the aim error at each element can be obtained as:

$$(\|e_D\|_i)_{\text{aim}} = \frac{1}{\sqrt{m}} \|\widehat{D}\| \theta_{\text{aim}}. \quad (24)$$

The rate of convergence of local error depends on the order of elements. Thus, the new element size can be evaluated as:

$$(h_i)_{\text{new}} = \left[\frac{(\|e_D\|_i)_{\text{aim}}}{(\|e_D\|_i)_{\text{old}}} \right]^{1/p} (h_i)_{\text{old}}, \quad (25)$$

where h is the average element size and p is the order of element. To obtain the nodal element size, a simple averaging between elements joining a node is used.

Data Transfer Operator

In the nonlinear FE analysis, the new mesh must be used starting from the end of previous load step since the solution is history-dependent in nonlinear problems. Thus, the state and internal variables need to be mapped from the old finite element mesh to the new one. The process of data transfer can be carried out in three steps [44,45]. In the first step the continuous internal variables are obtained by projecting the Gauss point components to the nodal values using the 3D weighted-SPR method. In the second step, the nodal values of internal variables of old mesh are transferred to the nodes of new mesh. For this purpose, we must first determine which element in the old mesh contains the nodal point in the new finite element mesh. The nodal components in the old mesh are then transferred to the nodes of new mesh by applying the old shape functions of old elements and the global coordinates of the new nodes. The components of internal variables at the Gauss points of new mesh are finally obtained by interpolation using the shape functions of elements of the new mesh. These three steps are illustrated schematically in Figure 3.

Consider that a state array $\mathbf{\Lambda}_n^{\text{old}} = \left(\mathbf{u}_n^{\text{old}}, \boldsymbol{\varepsilon}_n^{\text{old}}, (\boldsymbol{\varepsilon}_n^p)^{\text{old}}, \boldsymbol{\sigma}_n^{\text{old}}, D_n^{\text{old}}\right)$ denote the values

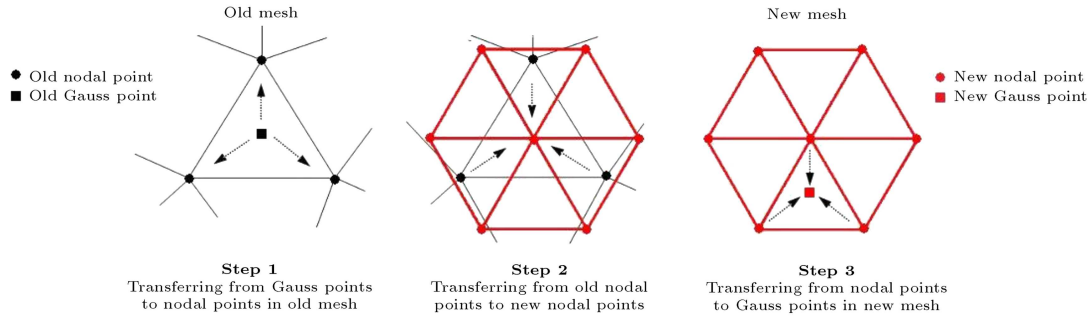

Figure 3. Three-step procedure of the transfer operator.

of displacement, strain tensor, plastic strain tensor, stress tensor and damage variable at time t_n for the mesh $\mathcal{M}_h$. Also assume that the estimated error of the solution $\mathbf{\Lambda}_n^{\text{old}}$ respects the prescribed criteria, while these are violated by the solution $\mathbf{\Lambda}_{n+1}^{\text{old}}$. In this case, a new mesh $\mathcal{M}_{\mathcal{H}}$ is generated and a new solution $\mathbf{\Lambda}_{n+1}^{\text{new}}$ is computed by evaluating the stress tensor $\boldsymbol{\sigma}_n^{\text{new}}$ and the damage variable D_n^{new} for a new mesh $\mathcal{M}_{\mathcal{H}}$ at time step t_n. In this way, the state array $\widehat{\mathbf{\Lambda}}_n^{\text{new}} = (\boldsymbol{\sigma}_n^{\text{new}}, D_n^{\text{new}})$ is constructed, where $\widehat{\mathbf{\Lambda}}$ is used to denote a reduced state array. It must be noted that the state array $\widehat{\mathbf{\Lambda}}$ characterizes the history of the material and provides sufficient information for computation of a new solution $\mathbf{\Lambda}_{n+1}^{\text{new}}$. The aim is to transfer the internal variables $((\boldsymbol{\sigma}_n)_G^{\text{old}}, (D_n)_G^{\text{old}})$ stored at the Gauss points of the old mesh $\mathcal{M}_h$ to the Gauss points of new mesh $\mathcal{M}_{\mathcal{H}}$. The transfer operator $\mathcal{T}_1$ between meshes $\mathcal{M}_h$ and $\mathcal{M}_{\mathcal{H}}$ can be defined as:

$$((\boldsymbol{\sigma}_n)_G^{\text{new}}, (D_n)_G^{\text{new}}) = \mathcal{T}_1[(\boldsymbol{\sigma}_n)_G^{\text{old}}, (D_n)_G^{\text{old}}]. \tag{26}$$

The variables $((\boldsymbol{\sigma}_n)_G^{\text{old}}, (D_n)_G^{\text{old}})$ specified at Gauss points of the mesh $\mathcal{M}_h$ are transferred by the operator $\mathcal{T}_1$ to each point of the domain Ω, in order to specify the variables $((\boldsymbol{\sigma}_n)_G^{\text{new}}, (D_n)_G^{\text{new}})$ at the Gauss points of new mesh $\mathcal{M}_{\mathcal{H}}$. The operator $\mathcal{T}_1$ can be constructed by a least-squares method, or a suitable projection technique.

In order to obtain the continuous values of stress tensor and damage variable $\widehat{\mathbf{\Lambda}}_n^{\text{old}} = ((\boldsymbol{\sigma}_n)^{\text{old}}, D_n^{\text{old}})$, the Gauss point components $(\boldsymbol{\sigma}_n)_G^{\text{old}}$ and $(D_n)_G^{\text{old}}$ are projected to nodal points to evaluate the components $(\boldsymbol{\sigma}_n)_N^{\text{old}}$ and $(D_n)_N^{\text{old}}$. In this study, the projection of the Gauss point components to the nodal points is carried out using the weighted-SPR technique, as described in previous section. The nodal components of the stress tensor $(\boldsymbol{\sigma}_n)_N^{\text{old}}$ and the damage variable $(D_n)_N^{\text{old}}$ for the mesh $\mathcal{M}_h$ are then transferred to the nodes of the new mesh $\mathcal{M}_{\mathcal{H}}$ resulting in components $(\boldsymbol{\sigma}_n)_N^{\text{new}}$ and $(D_n)_N^{\text{new}}$. The components of stress tensor and damage variable at the Gauss points of the new mesh $\mathcal{M}_{\mathcal{H}}$, i.e. $(\boldsymbol{\sigma}_n)_G^{\text{new}}$ and $(D_n)_G^{\text{new}}$, are finally obtained by using the interpolation of the shape functions of the new finite elements. In this procedure, the local coordinates are used to interpolate the variables from the nodes of mesh $\mathcal{M}_h$ to the nodes of mesh $\mathcal{M}_{\mathcal{H}}$. In the case of linear four-noded tetrahedral element, the local coordinates are obtained by solving a linear system of algebraic equations. In the case of higher order elements, the problem becomes nonlinear and the Newton-Raphson iterative scheme is implemented to obtain the local coordinates.

NUMERICAL SIMULATION RESULTS

In order to illustrate the accuracy and robustness of the proposed adaptive finite element method in three-dimensional damage mechanics, several problems are simulated numerically. Two benchmark examples are chosen to evaluate the performance of adaptive FE strategy for the crack initiation in a cylindrical pre-notched bar and a finite crack in the 3D rectangular specimen. In order to tackle 3D damage mechanics problems the proposed adaptive FE method is implemented in the computer software SUT-DAM, which was designed by the senior author in [46-48] for adaptive mesh refinement of large plasticity deformations and has been extended to adaptive analysis of damage growth simulation. The ten-noded tetrahedral elements are employed for the finite element meshes, and the numerical integration is carried out using four Gauss-Legendre quadrature points. The projection of the values of Gauss points to nodal points is carried out by using the 3D weighted-SPR method. The stress tensor and damage variable are mapped from the old mesh to new one during the data transfer process. The Lemaitre coupled plasticity-damage model is used in conjunction with the micro-crack closure effect to predict the damage growth in specimens. In order to solve the nonlinear equation systems, the global stiffness matrix is formed at the first iteration of each loading increment, and remains unchanged during iterations afterwards, i.e. the modified Newton-Raphson iterative procedure is employed. In all examples, the results are compared with those reported by previous researches.

Crack Initiation in a Cylindrical Pre-notched Bar

The first example is of a classical tensile test of a cylindrical pre-notched bar which has been extensively used by various researchers [49-52]. The geometry and boundary conditions of the specimen are shown in Figure 4. On the virtue of symmetry, only one-eighth of the problem is modeled. The specimen is subjected to the tensile prescribed displacement at the top edge. The bar is constructed by a low carbon steel in a rolled state with the following material properties: $E = 210$ GPa and $\nu = 0.3$. The strain hardening is considered to be isotropic and its curve has an exponential form governed by:

$$\boldsymbol{\sigma}_Y = 620 + 3300[1 - \exp(-0.4\varepsilon^p_{eq})] \qquad \text{(MPa)}, \qquad (27)$$

where ε^p_{eq} is the equivalent plastic strain. The parameters of Lemaitre model were calibrated by Benallal et al. [53] for this specimen given as $s = 1.0$ and $r = 3.5$ MPa. This specimen was also simulated by de Souza Neto et al. [33] using 2D FE modeling to validate the performance of their constitutive model in damage mechanics. The vertical displacement is applied incrementally in 600 increments of 0.001 mm. The damage evolution is predicted by Lemaitre model until its value reaches to the critical damage value of $D_C = 0.99$.

In Figure 5, the distribution of damage contours are shown at three stages and compared with those reported by de Souza Neto et al. [33] in two-dimensional modeling. It can be seen that the predicted damage contours are in good agreement with those obtained in [33]. It is interesting to note that the location of maximum damage is not fixed in the model and moves at different stages of loading. It can be observed that the maximum damage occurs in the outer part of the specimen at the first stages of loading, however, it moves toward the center of the bar by increasing the load. This can be justified by the fact that at early

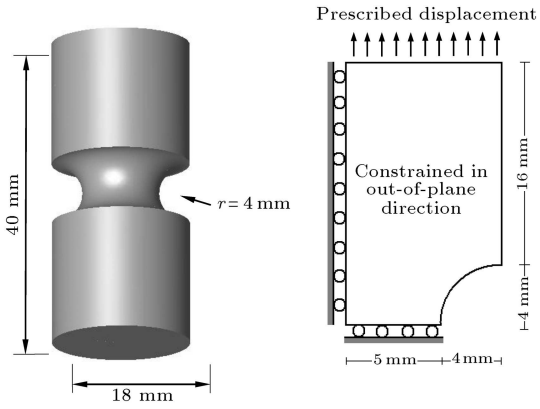

Figure 4. The cylindrical notched specimen; the geometry and boundary conditions.

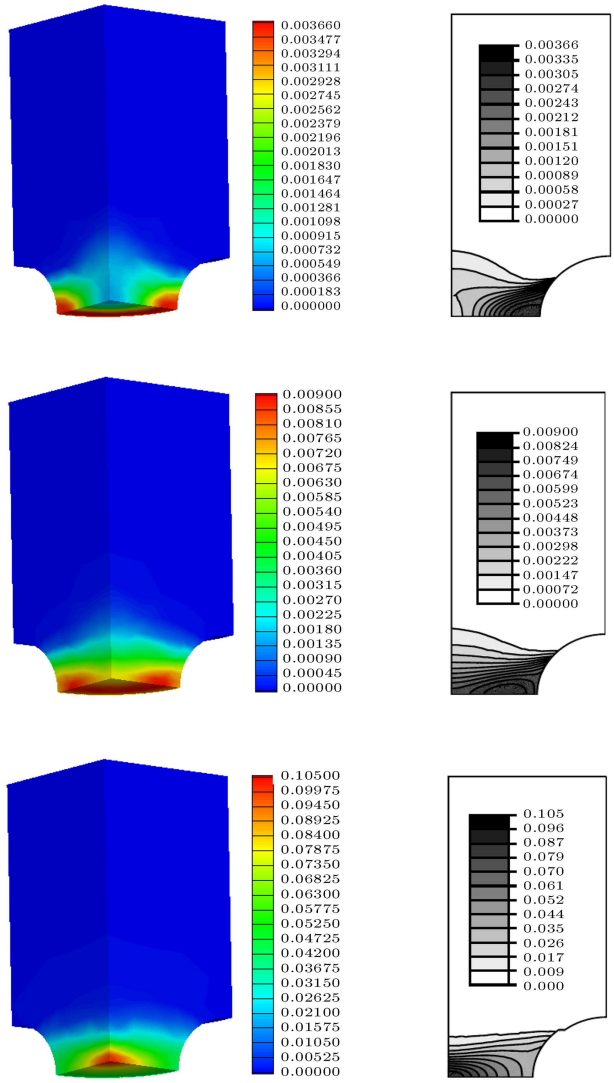

Figure 5. The distribution of damage contours at various load steps. A comparison between the present 3D model and 2D result reported by de Souza Neto et al. [33].

stages of loading the hydrostatic stress is low and the damage evolution is affected by the plastic flow. Thus, the damage grows in outer layers where the maximum equivalent plastic strain occurs. However, by increasing the load, the hydrostatic stress increases and its effect becomes dominant. Hence, the damage critical point moves toward the center of the bar where the maximum value of hydrostatic stress occurs. This phenomenon is also observed experimentally by Hancock and Mackenzie [54] where the failure of the bar initiates from the center of the bar. A comparison of the damage variable evolution at the centre of the specimen between the present study and 2D results reported by de Souza Neto et al. [33] is shown in Figure 6. The rate of damage growth is proportional to the damage value itself. In Figure 7, the variation of reaction force is plotted with the prescribed displacement. In order to control the

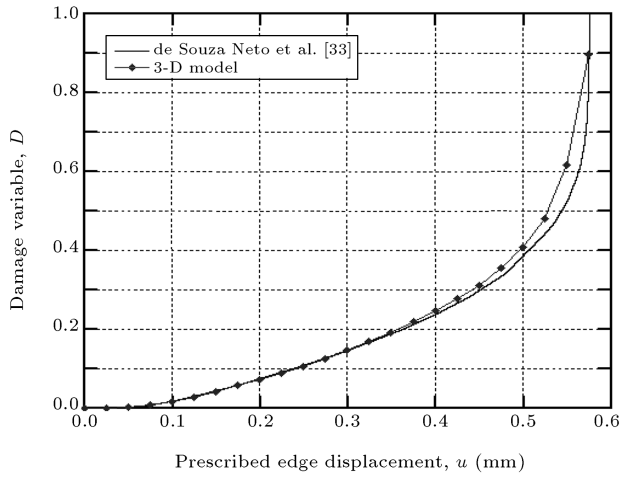

Figure 6. The damage variable evolution at the centre of specimen. A comparison between the present 3D model and 2D result reported by de Souza Neto et al. [33].

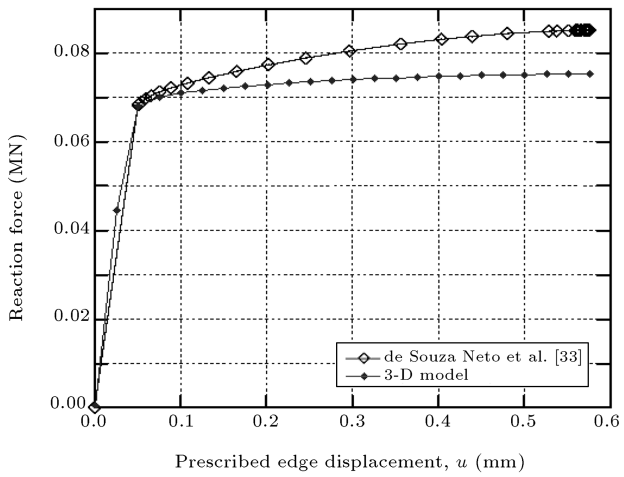

Figure 7. The force-displacement diagram for the cylindrical notched specimen. A comparison between the present 3D model and 2D result reported by de Souza Neto et al. [33].

error of the solution, an adaptive FE mesh refinement is carried out to generate the optimal mesh. The weighted superconvergent patch recovery technique is used with the aim error of 5%. This process is carried out at two steps of 50 and 360, as shown in Figure 8. This figure clearly presents the distribution of elements on the specimen with the growth of damage. In Figure 9, the effect of adaptive strategy can be observed on the estimated error. Obviously, the adaptive mesh refinements result in a reduced estimated error and converge to the prescribed target error.

A Finite Crack in a 3D Rectangular Specimen

The second example illustrates the damage growth in mode-I loading condition of a three-dimensional

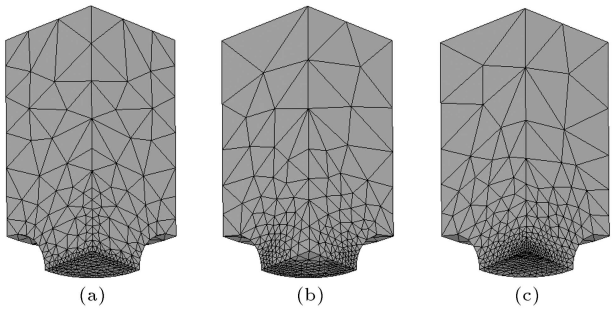

Figure 8. Adaptive mesh refinement technique for the cylindrical notched specimen. a) Initial FE mesh; b) adapted mesh at $u = 0.05$ mm; and c) adapted mesh at $u = 0.36$ mm.

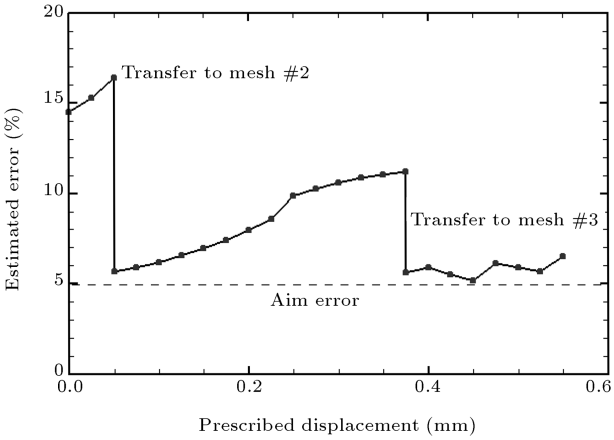

Figure 9. The variation of estimated error with prescribed displacement during adaptive mesh refinement.

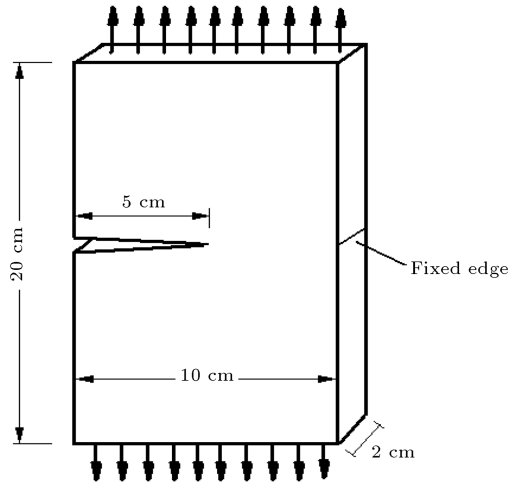

Figure 10. A 3D rectangular specimen with finite crack; the geometry and boundary conditions.

rectangular specimen of $20 \times 10 \times 2$ cm with a finite crack, as shown in Figure 10. This example is chosen to validate the accuracy of proposed adaptive FE algorithm for a benchmark problem. The 3D specimen is subjected to the prescribed displacement until the

damage variable reaches to the critical value $D_C = 0.95$. This condition was attained for a prescribe displacement of $u = 1.1$ mm. This example was proposed by Chung et al. [55] to verify the ability of their two-step parallel computing technique. The model is made by an aluminum alloy with the material properties given in Table 1. The strain hardening of material is governed by the following exponential function, i.e.:

$$\boldsymbol{\sigma}_Y = h_1 \boldsymbol{\varepsilon}^p_{eq} + (h_1 - h_0)\exp(-m\boldsymbol{\varepsilon}^p_{eq})/m. \tag{28}$$

In Figure 11, the distribution of damage contours are shown at various load steps and compared with those reported by Chung et al. [55]. Complete agreement can be observed between two numerical simulations. Obviously, the critical damage point is obtained at the crack tip and the crack growth is expected to initiate from this point. The distribution of damage is also symmetric around the crack tip. The magnitude of maximum damage obtained by the present simulation and that reported by Chung et al. [55] are plotted in Figure 12. The discrepancy between two numerical simulations can be related to the different damage models used in these simulations, and the calibration performed for obtaining the parameters of two damage models. In Figure 13, the initial FE mesh is shown together with the adaptive mesh refinements obtained using the weighted-SPR technique for the damage modeling. It must be noted that the finest adapted FE mesh used in present simulation has 30000 degrees-of-freedom, while the finite element mesh used in reference [55] was taken more than one million DOFs to achieve an acceptable result. The process of error estimation is carried out in this example at two stages and the results are plotted in Figure 14. Obviously, the adaptive mesh refinement procedure reduces the estimated error considerably.

Table 1. Mechanical properties and material constants of aluminum alloy.

Material Constant	Parameter	Value
Young modulus	E	72.4 GPa
Poisson ratio	ν	0.32
Hardening constant	m	25
Initial hardness constant	h_0	1150 MPa
Ultimate hardness constant	h_1	1670 MPa
Damage constant 1	s	1.0
Damage constant 2	r	1.5 MPa

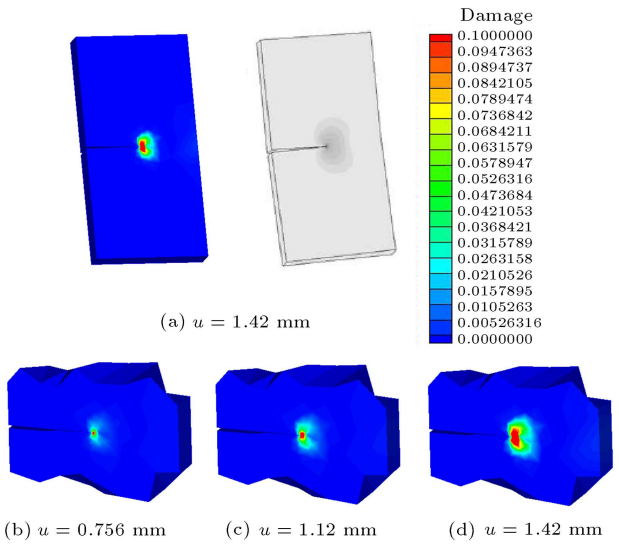

Figure 11. a) A comparison of final damage contours between the present model and that reported by Chung et al. [55]; and (b-d) damage contours near the crack tip at various load steps.

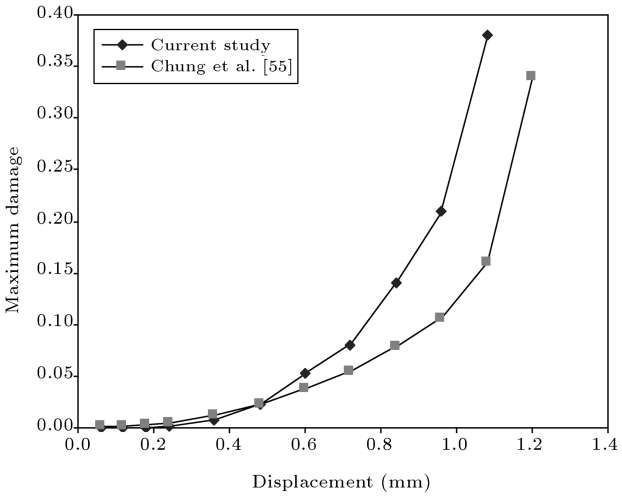

Figure 12. The evolution of damage variable at crack tip for the 3D tensile specimen; a comparison between the present model and that reported by Chung et al. [55].

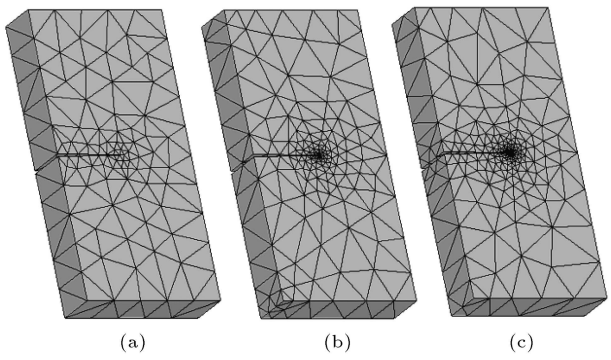

Figure 13. Adaptive mesh refinement model for the 3D tensile specimen. a) Initial FE mesh; b) adapted mesh at $u = 0.4$ mm; and c) adapted mesh at $u = 0.8$ mm.

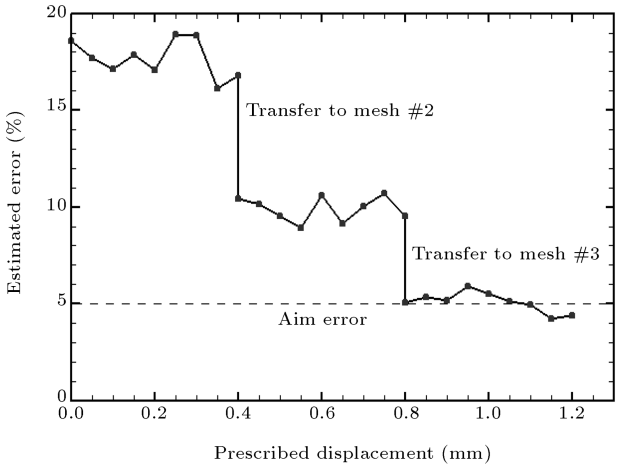

Figure 14. The variation of estimated error with prescribed displacement during adaptive mesh refinement.

A Knee-Lever with a Corner Crack

The last example is of a knee-lever connection, which is extensively used for machine systems. The component has an initial crack in the symmetric plane and oriented perpendicular to the adjacent surfaces. The crack edge has a circular shape with a radius of 5 mm. The connection is loaded by the prescribed displacement in two edge holes simultaneously and restrained at the middle hole. The geometry and boundary conditions of this component are shown in Figure 15. In Figure 16 the location of corner crack is shown in the three-dimensional view. The connection is made of the aluminum alloy AlZnMgCu 1.5 which is a proper choice in lightweight structures for its high ratio of strength to density. The elasticity modulus of specimen is $E = 32.5$ GPa and the Poisson ratio is $\nu = 0.3$. The

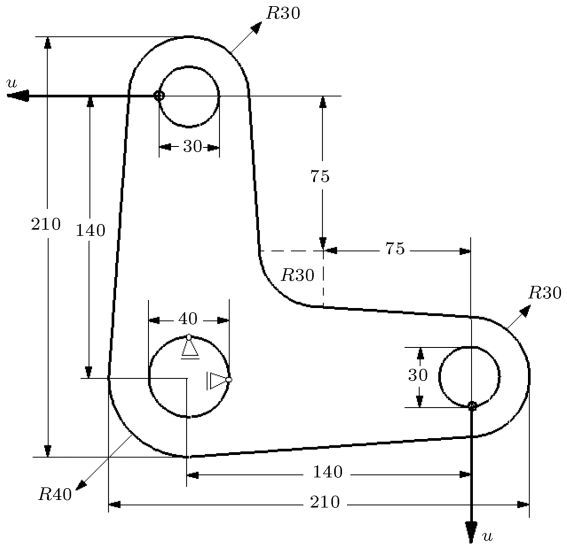

Figure 15. A knee-lever with a corner crack; the geometry and boundary conditions (all dimensions in mm).

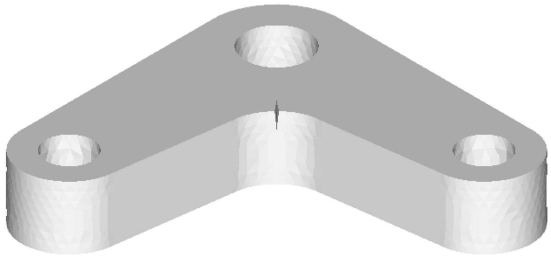

Figure 16. A knee-lever with a corner crack; the crack geometry.

initial yield stress is assumed to be $\sigma_{Y0} = 350$ MPa and the material hardening is governed by a linear hardening of $H = 820$ MPa. Schollmann et al. [56] simulated this component to illustrate the capabilities of their software in handling complex structures and crack under fatigue loading. To emphasize on three-dimensional behavior of component, the thickness of the specimen is increased here from 15 mm to 40 mm.

Based on the Lemaitre damage model with no micro-crack closure effect, the maximum damage occurs at loading points of edge holes because of high compression stresses at these regions. However, by introducing this effect to the model, the critical damage transmits to the crack tip region, as demonstrated in Figure 17. As can be observed from this figure, the crack tip in the thickness direction illustrates the higher damage than the crack tip in the upper surface of the component. Thus, the crack first grows in the thickness direction and then penetrates in the depth of component. This observation can be verified with that reported by Schollmann et al. [56]. Figure 18 displays the reaction force versus prescribed displacement for the knee-lever connection. In Figure 19 the maximum damage variable evolution at different displacements is plotted. It can be observed that the damage growth starts at prescribed displacement of 1 mm and rapidly reaches to its critical value at displacement of 2 mm, however, the crack tip region reaches the critical damage at displacement of 9 mm. Furthermore, the critical damage point is obtained at the front crack tip during loading steps, since both the hydrostatic stress and effective plastic strain are concentrated on this point. During the damage growth process, two

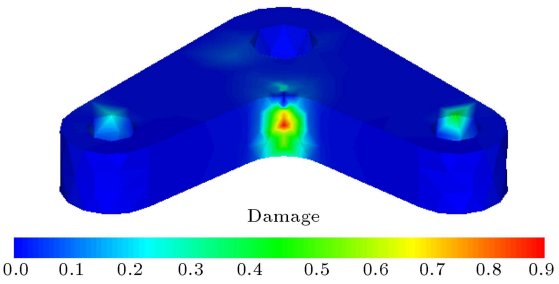

Figure 17. The damage contour for a knee-lever with a corner crack.

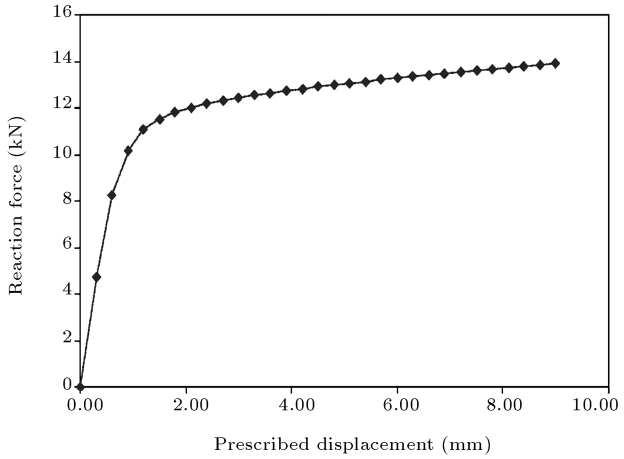

Figure 18. The force-displacement curve for a knee-lever with a corner crack.

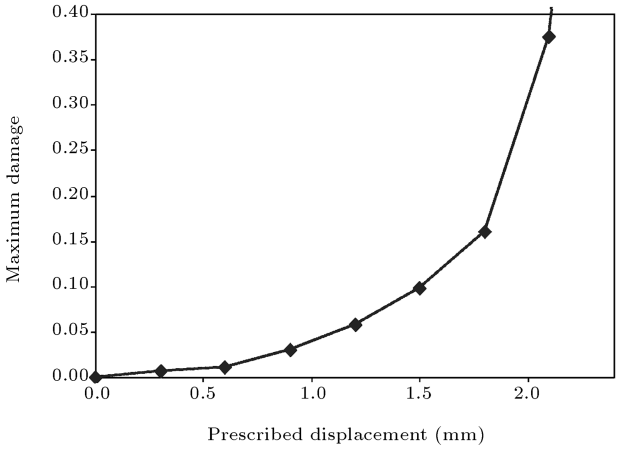

Figure 19. The evolution of damage variable at crack tip.

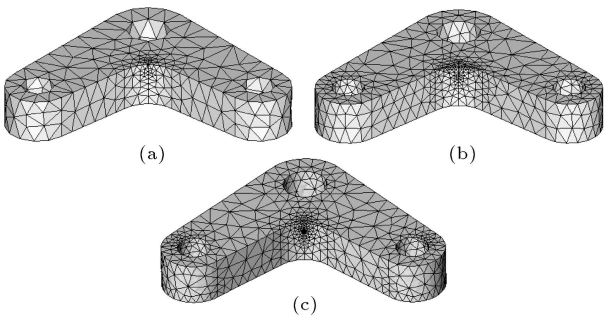

Figure 20. The adaptive mesh refinement strategy for a knee-lever with a corner crack. a) Initial FE mesh, b) adapted mesh at $u = 1.15$ mm, c) adapted mesh at $u = 6.10$ mm.

successive mesh refinements with the aim error of 5% are performed. In Figure 20, the initial and adapted FE meshes are shown at $u = 1.15$ and 6.10 mm. The adaptive mesh refinement is performed at the start of damage growth and when the estimated error exceeds 10%. The effect of adaptive mesh refinement

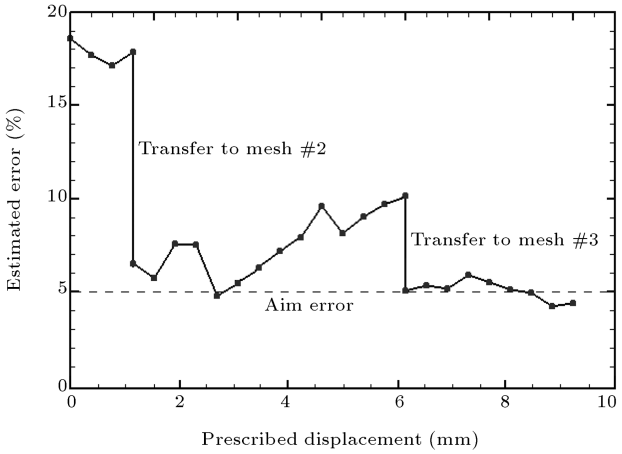

Figure 21. The variation of estimated error with prescribed displacement during adaptive mesh refinement.

is obvious in the variation of estimated error at the damage growth process, as shown in Figure 21.

CONCLUSION

In the present paper, an adaptive finite element method was presented for the three-dimensional analysis of damage growth and crack initiation. The formulation takes into account the micro-crack closure effect on damage evolution, to distinguish between the tensile and compressive stresses. The constitutive modeling was implemented within the framework of continuum damage mechanics. A simplified version of Lemaitre damage model was employed to estimate the damage evolution. The adaptive finite element technique was implemented through the following three stages: an error estimation, adaptive mesh refinement and data transferring. The error estimation procedure was used based on the Zienkiewicz-Zhu error estimator and a weighted superconvergent patch recovery technique was employed. The accuracy and robustness of proposed computational algorithm in 3D damage mechanics were presented by three numerical examples. The results clearly show the ability of the model in capturing the damage growth and crack initiation in two benchmark examples and a complex 3D problem. In a later work, we will show how the proposed technique can be used in a 3D automatic simulation of crack propagation in the fracture of ductile materials.

REFERENCES

1. Kachanov, L.M. "Time of the rupture process under creep condition", *Izvestiya Akademii Nauk SSSR*, Otdeleniya Tekhnika Nauk., **8**, pp. 26-31 (1958).
2. Rice, J.R. and Tracy, D.M. "On ductile enlargement of voids in triaxial stress fields", *Journal of Mechanics and Physics of Solids*, **17**, pp. 210-217 (1969).
3. Gurson, A.L. "Continuum theory of ductile rupture by

void nucleation and growth - Part I: Yield criteria and flow rule for porous media", *Journal of Engineering Materials and Technology*, **99**, pp. 2-15 (1977).

4. Murakami, S. and Ohno, N. "A continuum theory of creep and creep damage", *Proceedings of the IUTAM Symposium on Creep in Structures*, Leicester (1981).
5. Lemaitre, J. "A continuous damage mechanics model for ductile fracture", *Journal of Engineering Materials and Technology*, **107**, pp. 83-89 (1985).
6. Chow, C.L. and Wang, J. "An anisotropic theory of continuum damage mechanics for ductile fracture", *Engineering Fracture Mechanics*, **27**, pp. 547-558 (1987).
7. Lemaitre, J. and Chaboche, J.L., *Mechanics of Solid Materials*, Cambridge University Press (1990).
8. Peerlings, R.H.J., De Borst, R., Brekelmans, W.A.M. and De Vree J.H.P. "Gradient enhanced damage for quasi-brittle materials", *International Journal for Numerical Methods in Engineering*, **39**, pp. 3391-3403 (1996).
9. Pardoen, T. "Numerical simulation of low stress triaxiality ductile failure", *Computer and Structures*, **84**, pp. 1641-1650 (2006).
10. Hambli, R. "Comparison between Lemaitre and Gurson damage models in crack growth simulation during blanking process", *International Journal of Mechanical Sciences*, **43**, pp. 2769-2790 (2001).
11. Areias, P.M.A. and Belytschko, T. "Analysis of three-dimensional crack initiation and propagation using the extended finite element method", *International Journal for Numerical Methods in Engineering*, **63**, pp. 760-788 (2005).
12. Grassl, P. and Jirasek, M. "Damage-plastic model for concrete failure", *International Journal of Solids and Structures*, **43**, pp. 7166-7196 (2006).
13. Mediavilla, J., Peerlings, R.H.J. and Geers, M.G.D. "An integrated continuous-discontinuous approach towards damage engineering in sheet metal forming processes", *Engineering Fracture Mechanics*, **73**, 895-916 (2006).
14. Comi, C., Mariani, S. and Perego, U. "An extended FE strategy for transition from continuum damage to mode I cohesive crack propagation", *International Journal for Numerical and Analytical Methods in Geomechanics*, **31**, pp. 213-238 (2007).
15. Verfurth, R. "A review of a posteriori error estimation techniques for elasticity problems", *Computer Methods in Applied Mechanics and Engineering*, **176**, pp. 419-440 (1999).
16. Diez, P. and Huerta, A. "A unified approach to remeshing strategies for finite element h-adaptivity", *Computer Methods in Applied Mechanics and Engineering*, **176**, pp. 215-229 (1999).
17. Zienkiewicz, O.C. and Zhu, J.Z. "A simple error estimator and adaptive procedure for practical engineering analysis", *International Journal for Numerical Methods in Engineering*, **24**, pp. 337-357 (1987).
18. Babuska, I. and Rheinboldt, W.C. "A posteriori error estimates for the finite element method", *International Journal for Numerical Methods in Engineering*, **12**, 1597-1615 (1978).
19. Zienkiewicz, O.C. and Zhu, J.Z. "The superconvergent patch recovery and a posteriori error estimates. Part I: The recovery technique", *International Journal for Numerical Methods in Engineering*, **33**, pp. 1331-1364 (1992).
20. Zienkiewicz, O.C. and Zhu, J.Z. "The superconvergence patch recovery and a posteriori error estimates. Part II: Error estimates and adaptivity", *International Journal for Numerical Methods in Engineering*, **33**, pp. 1365-1380 (1992).
21. Boroomand, B. and Zienkiewicz, O.C. "Recovery procedures in error estimation and adaptivity. Part II: Adaptivity in nonlinear problems of elasto-plasticity behavior", *Computer Methods in Applied Mechanics and Engineering*, **176**, pp. 127-146 (1999).
22. Wiberg, N.E., Abdulwahab, F. and Ziukas, S. "Enhanced superconvergent patch recovery incorporating equilibrium and boundary conditions", *International Journal for Numerical Methods in Engineering*, **37**, pp. 3417-3440 (1994).
23. Gu, H., Zong, Z. and Hung, K.C. "A modified superconvergent patch recovery method and its application to large deformation problems", *Finite Elements in Analysis and Design*, **40**, pp. 665-687 (2004).
24. Bugeda, G. "A new adaptive remeshing scheme based on the sensitivity analysis of the SPR point wise error estimation", *Computer Methods in Applied Mechanics and Engineering*, **195**, pp. 462-478 (2006).
25. Khoei, A.R. and Gharehbaghi, S.A. "The superconvergence patch recovery and data transfer operators in 3D plasticity problems", *Finite Elements in Analysis and Design*, **43**, pp. 630-648 (2007).
26. Khoei, A.R. and Gharehbaghi, S.A. "Three-dimensional data transfer operators in plasticity using SPR technique with C_0, C_1 and C_2 continuity", *Scientia Iranica*, **15**, pp. 554-567 (2008).
27. Khoei, A.R., Azadi, H. and Moslemi, H. "Modeling of crack propagation via an automatic adaptive mesh refinement based on modified superconvergent patch recovery technique", *Engineering Fracture Mechanics*, **75**, pp. 2921-2945 (2008).
28. Moslemi, H. and Khoei, A.R. "3D adaptive finite element modeling of non-planar curved crack growth using the weighted superconvergent patch recovery method", *Engineering Fracture Mechanics*, **76**, pp. 1703-1728 (2009).
29. Khoei, A.R., Moslemi, H., Majd Ardakany, K., Barani O.R. and Azadi, H. "Modeling of cohesive crack growth using an adaptive mesh refinement via the modified-SPR technique", *International Journal of Fracture*, **159**, pp. 21-41 (2009).
30. Lemaitre, J. and Chaboche, J.L. *Mecanique de Materiaux Solides*, Dunod, Paris (1985).

31. Benallal, A., Billardon, R. and Doghri, I. "An integration algorithm and the corresponding consistent tangent operator for fully coupled elastoplastic and damage equations", *Communications in Applied Numerical Methods*, **4**, pp. 731-740 (1988).

32. Steinmann, P., Miehe, C. and Stein, E. "Comparison of different finite deformation inelastic damage models within multiplicative elastoplasticity for ductile metals", *Computational Mechanics*, **13**, pp. 458-474 (1994).

33. de Souza Neto, E.A., Peric, D. and Owen, D.R.J., *Computational Methods for Plasticity: Theory and Applications*, Wiley, UK (2008).

34. Ladevèze, P. "Sur une théorie de l'endommagement anisotrope", Technical Report 34, Laboratoire de Mécanique et Technologie, Ecole Normale Supérieure de Cachan (1983).

35. Desmorat, R. "Quasi-unilateral conditions in anisotropic elasticity", *Comptes Rendus de l'Academie de Sciences - Serie IIb: Mecanique*, **328**, pp. 445-450 (2000).

36. Halm, D. and Dragon, A. "A model of anisotropic damage by mesocrack growth: unilateral effect", *International Journal of Damage Mechanics*, **5**, pp. 384-402 (1996).

37. La Borderie, C. "Phénomènes unilatéraux dans un matériau endommageable: Modélisation et application à l'analyse de structures en béton", Thèse de doctorat, Université Paris 6, Ecole Normale Supérieure de Cachan; mai (1991).

38. Murakami, S. and Kamiya, K. "Constitutive and damage evolution equations of elastic brittle materials based on irreversible thermodynamics", *International Journal of Mechanical Science*, **39**, pp. 473-486 (1997).

39. Kuna-Ciskal, H. and Skrzypek, J. "CDM based modelling of damage and fracture mechanisms in concrete under tension and compression", *Engineering Fracture Mechanics*, **71**, pp. 681-698 (2004).

40. Challamel, N., Lanos, C. and Casandjian, C. "Strain-based anisotropic damage modelling and unilateral effects", *International Journal of Mechanical Science*, **47**, pp. 459-473 (2005).

41. Arnold, G., Hubert, O., Dutko, M. and Billardon, R. "Identification of a continuum damage model from micro-hardness measurements", *International Journal of Forming Processes*, **5**, pp. 163-173 (2002).

42. Gago, J.P., Kelly, D.W. and Zienkiewicz, O.C. "Posteriori error analysis and adaptive processes in the finite element method. Part II: adaptive mesh refinement", *International Journal for Numerical Methods in Engineering*, **19**, pp. 1621-1656 (1983).

43. Kelly, D.W. "The self-equilibration of residuals and complementary a posteriori error estimates in the finite element method", *International Journal for Numerical Methods in Engineering*, **20**, pp. 1491-1506 (1984).

44. Gharehbaghi, S.A. and Khoei, A.R. "Three-dimensional superconvergent patch recovery method and its application to data transferring in small strain plasticity", *Computational Mechanics*, **41**, pp. 293-312 (2008).

45. Khoei, A.R. and Gharehbaghi, S.A. "Three-dimensional data transfer operators in large plasticity deformations using modified-SPR technique", *Applied Mathematical Modelling*, **33**, pp. 3269-3285 (2009).

46. Khoei, A.R., Tabarraie, A.R. and Gharehbaghi, S.A. "H-adaptive mesh refinement for shear band localization in elasto-plasticity Cosserat continuum", *Communication in Nonlinear Sciences and Numerical Simulation*, **10**, pp. 253-286 (2005).

47. Khoei, A.R., Gharehbaghi, S.A., Azami, A.R. and Tabarraie, A.R. "SUT-DAM: an integrated software environment for multi-disciplinary geotechnical engineering", *Advances Engineering Software*, **37**, pp. 728-753 (2006).

48. Khoei, A.R., Gharehbaghi, S.A., Tabarraie, A.R. and Riahi, A. "Error estimation, adaptivity and data transfer in enriched plasticity continua to analysis of shear band localization", *Applied Mathematical Modeling*, **31**, pp. 983-1000 (2007).

49. Benallal, A., Billardon, R. and Lemaitre, J. "Continuum damage mechanics and local approach to fracture: Numerical procedures", *Computer Methods in Applied Mechanics and Engineering*, **92**, pp. 141-155 (1991).

50. Cescotto, S. and Zhu, Y.Y. "Modelling of ductile fracture initiation during bulk forming", *Computational Plasticity: Fundamentals and Applications*, Barcelona (1995).

51. Vaz, Jr. M. and Owen, D.R.J. "Aspects of ductile fracture and adaptive mesh refinement in damaged elasto-plastic materials", *International Journal for Numerical Methods in Engineering*, **50**, pp. 29-54 (2001).

52. Andrade Pires, F.M., de Souza Neto, E.A. and Owen, D.R.J. "On the finite element prediction of damage growth and fracture initiation in finitely deforming ductile materials", *Computer Methods in Applied Mechanics and Engineering*, **193**, pp. 5223-5256 (2004).

53. Benallal, A., Billardon, R., Doghri, I. and Moret-Bailly, L. "Crack initiation and propagation analyses taking into account initial strain hardening and damage fields", *Numerical Methods in Fracture Mechanics, Proceedings of the Fourth International Conference*, held in San Antonio, Texas (1987).

54. Hancock, J.W. and Mackenzie, A.C. "On the mechanism of ductile fracture in high-strength steels subjected to multi-axial stress-states", *Journal of Mechanics and Physics of Solids*, **24**, pp. 147-169 (1976).

55. Chung, S.W., Lee, C.S. and Kim, S.J. "Large-scale simulation of crack propagation based on continuum damage mechanics and two-step mesh partitioning", *Mechanics of Materials*, **38**, pp. 76-87 (2006).

56. Schollmann, M., Fulland, M. and Richard, H.A. "Development of a new software for adaptive crack growth simulations in 3D structures", *Engineering Fracture Mechanics*, **70**, pp. 249-268 (2003).

BIOGRAPHIES

H. Moslemi received his B.S. in Civil Engineering from Sharif University of Technology, in 2003, and his M.S. degree in Structural Engineering from University of Tehran, in 2005. He completed his Ph.D. in 2010 in Computational Mechanics under the supervision of Professor A.R. Khoei from Sharif University of Technology.

Dr Moslemi is currently an assistant professor in the Civil Engineering Department at Shahed University. His academic career also includes positions in a number of Iranian universities such as International Campus of Sharif University of Technology in Kish Island and Qazvin Islamic Azad University. His research interests include Computational Fracture Mechanics, Crack Propagation and Damage Mechanics.

Amir Reza Khoei received his Ph.D. in Civil Engineering from the University of Wales Swansea in UK in 1998. He is currently a professor in the Civil Engineering Department at Sharif University of Technology. He is the editor of Scientica Iranica, Transaction A, Journal of Civil Engineering, a member of the editorial board of the Journal of Science and Technology (Sharif University of Technology), and the co-editor of the 11th International Symposium on Plasticity and Its Current Application in US, 2005. Dr Khoei has selected as a distinguished researcher at Sharif University of Technology in 2003, 2005, 2007 and 2008, and as a distinguished professor by the Ministry of Science, Research and Technology in 2008. He is the silver medal winner of Khwarizmi International Award (2005) organized by the Iranian Research Organization for Science and Technology.